JOURNAL OF COMPUTATIONAL PHYSICS 98, 317–331 (1992)

Time-Implicit Fluid Simulation of Collisional Plasmas

P. W. RAMBO AND J. DENAVIT

University of California, Lawrence Livermore National Laboratory, Livermore, California 94550

Received July 13, 1990; revised January 28, 1991

A one-dimensional algorithm for fluid simulation of interpenetrating multi-component plasmas, developed earlier for the collisionless case [1], is extended to include collisions between species. The finite-differenced fluid equations, including collision forces, are coupled with the Poisson equation to give time-implicit solutions, which are stable and accurate over a wide range of the time scale parameters $\omega_p \Delta t$ and $\nu_c \Delta t$ (ω_p is the plasma frequency, ν_c is a typical collision frequency, and Δt is the time step). In regions where $\omega_p \Delta t \ll 1$ and $\nu_c \Delta t \ll 1$, electron dynamics and space-charge effects are resolved, while in regions where $\omega_p \Delta t \gg 1$ and/or $\nu_c \Delta t \gg 1$, the ambipolar and/or diffusion models are recovered. Results of tests are presented, including ohmic heating, shocks with an interface between different fluids, colliding plasmas in which a region of interpenetrating fluids is created, and plasma shocks with separate electron and ion fluids.

I. INTRODUCTION

There is growing interest in fluid–particle hybrid simulations of plasmas, in which the dense-cold plasma components are treated using fluid models, while the sparse-energetic components are represented as particles [2, 3]. This interest is motivated by the need to model surface interactions between an energetic plasma or beam and electrodes or sheaths, with density ratios of several orders of magnitude. Such interactions play a role, for example, in electron and ion sources, diode closure, probe theory, and plasma processing of surfaces. The fluid algorithms used in such simulations must satisfy the following requirements:

(a) They must represent multiple interpenetrating fluids, consisting of electrons, ions and neutral fluids, interacting with each other via the electric field and collision forces.

(b) Since a given fluid component generally does not occupy the entire system, fluid–vacuum boundaries occur for each component. Such fluid–vacuum boundaries are found in interface regions between two fluid species, or between fluid and particle components. The fluid transport algorithm must give physically acceptable behavior at such boundaries.

(c) Electron inertia effects occurring at the time scale of the simulations must be included. This requires a time-implicit evaluation of the electric field giving stable and accurate numerical solutions for electron densities corresponding to a wide range of the time scale parameter $\omega_p \Delta t$. Here, $\omega_p = (4\pi e^2 n_e/m_e)^{1/2}$ is the plasma frequency, n_e is the electron density, e is the magnitude of the electron charge, m_e is the electron mass, and Δt is the time step. In low-density regions, where $\omega_p \Delta t \ll 1$, electron dynamics and space-charge effects must be resolved, while in high-density regions, where $\omega_p \Delta t \gg 1$, the numerical solution must give quasi-neutrality with an ambipolar electric field. In this limit of $\omega_p \Delta t \gg 1$, low frequency phenomena such as ion acoustic waves must still be correctly reproduced.

(d) The collisional coupling between fluid components must be represented over a wide range of the time scale parameter $\nu_c \Delta t$, where ν_c denotes any of the collision frequencies between fluid components. For $\nu_c \Delta t \ll 1$, the effect of friction on the dynamics of interpenetrating fluids must be modeled accurately, and for $\nu_c \Delta t \gg 1$, the solution must remain stable and reduce to Ohm's law (electron current proportional to electric field in uniform plasma) or to the diffusion model (momentum flux proportional to pressure gradient, hence $\partial n/\partial t \propto \partial^2 n/\partial x^2$ for neutral fluids) as appropriate. This requires simultaneous time-implicit solution of the collision forces between all fluid components present at a point [4].

A one-dimensional algorithm which meets these requirements for collisionless fluids was developed earlier [1]. In the present paper we extend this algorithm to include collision forces.

The multi-fluid formulation of Braginskii [5] is used with a set of fluid equations for each species, including electrons, ions, and neutral species. Dimensionless units are used with lengths measured in units of a characteristic length, λ_0. Velocity, particle mass, and temperature are measured in units of v_0, m_0, T_0, respectively, which are related by $v_0 = (T_0/m_0)^{1/2}$. Time is measured in units of λ_0/v_0. Particle density is in units of the characteristic density n_0, electric

0021-9991/92 $3.00

field in units of $E_0 = (4\pi n_0 T_0)^{1/2}$, and charge in units of the magnitude of the electron charge e.

The continuity and momentum equations for species s are

$$\frac{\partial n_s}{\partial t} + \frac{\partial}{\partial x}(n_s u_s) = 0 \tag{1}$$

and

$$\frac{\partial}{\partial t}[n_s u_s] + \frac{\partial}{\partial x}[n_s u_s^2] = n_s \dot{u}_s \tag{2}$$

with velocity source term

$$\dot{u}_s = -\frac{1}{m_s n_s}\frac{\partial}{\partial x}(n_s T_s) + \Omega_p \frac{q_s}{m_s} E - \frac{1}{m_s}\sum_{s'} m_{ss'} \nu_{ss'}[u_s - u_{s'}]. \tag{3}$$

Here n_s, u_s, T_s are the normalized number density, velocity, and temperature of fluid species s, E is the normalized electric field, q_s and m_s are the normalized charge and mass of species s and $m_{ss'} = m_s m_{s'}/(m_s + m_{s'})$. The quantity $\Omega_p = (4\pi n_0 e^2/m_0)^{1/2}\lambda_0/v_0$ is the dimensionless plasma frequency and is a measure of space charge effects. Collisions between species s and s' are defined by the collision frequencies $\nu_{ss'} = \alpha_{ss'} C_{ss'} n_{s'}$, where $\alpha_{ss'}$ denotes numerical constants of order unity and $C_{ss'}$ denotes symmetric coefficients which depend on the temperature. Both $\alpha_{ss'}$ and $C_{ss'}$ depend on the interaction force between particles during collisions (e.g., inverse square law for Coulomb collisions). The form of the coefficients $C_{ss'}$ is discussed in Appendix A. The electric field is obtained from the Poisson equation, which in these units takes the form

$$\frac{\partial E}{\partial x} = \Omega_p \sum_s q_s n_s. \tag{4}$$

The energy equation for species, s, is

$$\frac{\partial}{\partial t}(n_s T_s) + \frac{\partial}{\partial x}[u_s n_s T_s] = n_s \dot{T}_s, \tag{5}$$

where the temperature source, $\dot{T}_s$, is given by

$$\frac{3}{2}\dot{T}_s = -T_s\frac{\partial u_s}{\partial x} + \sum_{s'}\frac{m_{ss'}^2}{m_s}\nu_{ss'}[u_s - u_{s'}]^2 - \sum_{s' \neq s} B_{ss'} n_{s'}[T_s - T_{s'}] + \frac{1}{n_s}\frac{\partial}{\partial x}\kappa_s\frac{\partial T_s}{\partial x}. \tag{6}$$

The coefficient $\frac{3}{2}$ in Eq. (6) is appropriate for a monoatomic ideal gas with a ratio of specific heats, $\gamma = \frac{5}{3}$, $B_{ss'} = 3m_{ss'}C_{ss'}/(m_s + m_{s'})$, and κ_s denotes the flux limite heat conductivity as discussed in Appendix A.

An algorithm for the solution of the continuity an momentum equations, Eqs. (1)–(3), coupled with th Poisson equation, Eq. (4), is presented in Section II. A on dimensional uniform Eulerian mesh is considered with mes size Δx. This algorithm is an extension of Scheme 3 Ref. [1] to include collision forces. The numerical solutic of the energy equations, Eqs. (5), (6), is treated in Se tion III. A code implementing the algorithms of Sections and III, with an arbitrary number of species has bee written and tested on problems involving interactic between several fluids. These tests, presented in Section I include ohmic heating, shocks with an interface betwee separate fluids, colliding plasmas in which a region of inte penetrating fluids is created, and plasma shocks in whic electrons and ions are represented by separate fluids. Th collision coefficients $C_{ss'}$ and heat conductivities are discussed in Appendix A, and Appendix B defines th transport algorithm used in the numerical tests.

The code implementing these algorithms also allows fo creation and deletion of particles in regions of low coll sionality [2]. These particles are followed using particle-in cell techniques, which include scatter and drag due to coll sions with the fluids. These hybrid simulations, includin both fluids and particles will be described in a future pape but even without particles, this code follows the separa dynamics of the components of a mixture, rather than con sidering the mixture as a single fluid as typically done fluid plasma codes. This more detailed representation is pa ticularily important for the treatment of electrons and interfaces between fluids, where interpenetration of sever ion or neutral species can occur.

II. DENSITY, MOMENTUM, AND ELECTRIC FIELD

The numerical solution of the continuity and momentu equations, Eqs. (1)–(3), coupled with the time-implicit sol tion of the Poisson equation, Eq. (4), were studied Ref. [1] for the collisionless case. Three algorithms, ide tified as Schemes 1, 2, and 3, were examined. In Scheme all quantities, i.e., density, momentum, temperatur velocity, and electric field, are defined at cell centers ar Phoenical flux corrected transport is used [1]. This alg rithm gives good results at fluid–vacuum boundarie However, it yields a non-diagonal matrix for the implic solution of the electric field, which admits an unphysic even–odd mode in the electric field. This mode becom significant for $\omega_p \Delta t > 10$, seriously limiting the range allowed electron densities.

In Scheme 2, a staggered mesh is used, with density ar temperature defined at cell centers, while momentur velocity, and electric field are defined at cell boundarie

This algorithm yields a diagonal field solver, eliminating the even–odd mode in the electric field; but tests have shown that it gives poor results at fluid–vacuum boundaries.

Finally, in Scheme 3, density, momentum, and temperature are defined at cell centers, while velocity and electric field are defined at cell boundaries. This algorithm also yields a diagonal field solver, eliminating the even–odd mode in the electric field, and gives good results at fluid–vacuum boundaries. This Scheme 3 is now extended to include (a) momentum coupling between species due to collisions and (b) the effect of collisions on the implicit field solver.

Density and momentum are transported using a flux corrected method, such as the method of van Leer (see Eqs. (17) of Ref. [1]) or the algorithm described in Appendix B, which both use velocities at cell boundaries. A single transport step, such as advancing the cell-centered densities from their old values, n_j^0, to their new values, n_j^t, according to Eq. (1), is represented by the operator Ψ,

$$n_j^t = \Psi[n_j^0, u_{j+1/2}^t]. \tag{7}$$

Here, $u_{j+1/2}^t$, denotes the velocities at cell boundaries used to compute the fluxes in the transport algorithm. The superscript, t, implies using velocities at the new time level, but arbitrary time centering of the transport step may be achieved using a weighted average of velocities at the old and new time levels.

Momentum and velocity are advanced by first transporting the momentum according to Eq. (2), excluding the source term,

$$(nu)_j^* = \Psi[(nu)_j^0, u_{j+1/2}^t] \tag{8}$$

from which intermediary velocities at cell boundaries are calculated,

$$u_{j+1/2}^* = \frac{1}{2}\left[\frac{(nu)_j^*}{n_j^t} + \frac{(nu)_{j+1}^*}{n_{j+1}^t}\right]. \tag{9}$$

These velocities are then advanced by the source term contributions from Eq. (3). Including only the pressure and electric field contributions gives the collisionless velocity,

$$u_{j+1/2}^{\text{collisionless}} = u_{j+1/2}^* + \Delta t\left[-\frac{1}{m\langle n^t\rangle_{j+1/2}} \times \frac{P_{j+1}^t - P_j^t}{\Delta x} + \Omega_p \frac{q}{m} E_{j+1/2}^t\right], \tag{10}$$

where $\langle n^t\rangle_{j+1/2} = (n_{j+1}^t + n_j^t)/2$, and $P = nT + Q$ denotes the pressure including the artificial viscosity term Q[1].

a. *Collisional Momentum Coupling between Species*

The collisionless equations, Eqs. (7)–(10) can be applied separately to each species, while the contribution of the collision forces, which depend on the collision frequencies $\nu_{ss'}$ involve coupling between species. The algorithm representing this coupling and allowing large values of $\nu_{ss'}\,\Delta t$, may be understood in terms of the following simple example. Consider a single moving fluid, coupled by friction to a stationary background. For the spatially uniform case, where the density is constant and no pressure gradient or electric forces occur, the momentum equation reduces to

$$\frac{du}{dt} = -\nu_c u, \tag{11}$$

where ν_c is the collision frequency between the moving fluid and the stationary background. For constant collision frequency, the analytic solution is an exponential decay from the initial velocity, $u^t = u^0 \exp(-\nu_c t)$. In finite difference form, Eq. (11) may be written as

$$u^t - u^{t-\Delta t} = -\nu_c\,\Delta t\,[(1-\theta)\,u^{t-\Delta t} + \theta u^t]$$

or

$$u^t = \frac{1 + (\theta - 1)\,\nu_c\,\Delta t}{1 + \theta\nu_c\,\Delta t}\,u^{t-\Delta t}, \tag{12}$$

where θ is a time centering parameter, $0 \leqslant \theta \leqslant 1$, which controls the stability of the numerical solution for $\nu_c\,\Delta t \gg 1$. Three cases are considered:

(i) For $\theta = 0$, which corresponds to an explicit algorithm, Eq. (12) yields

$$u^t = (1 - \nu_c\,\Delta t)\,u^{t-\Delta t},$$

and for $\nu_c\,\Delta t \gg 1$, the solution is unstable as shown in Fig. 1a.

(ii) For $\theta = \frac{1}{2}$, which corresponds to a time-centered algorithm, Eq. (12) yields

$$u^t = \frac{1 - \nu_c\,\Delta t/2}{1 + \nu_c\,\Delta t/2}\,u^{t-\Delta t},$$

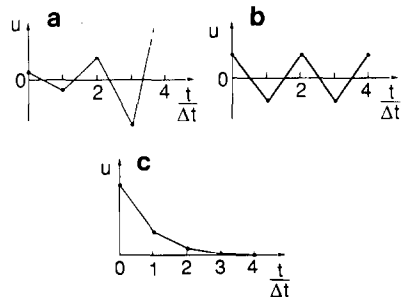

FIG. 1. Numerical solution of collisional slowing for $\nu_c\,\Delta t \gg 1$. (a) Explicit algorithm, $\theta = 0$, gives an unstable solution. (b) Time-centered algorithm, $\theta = \frac{1}{2}$, gives an oscillatory solution. (c) Implicit algorithm, $\theta = 1$, gives stable decay.

and for $\nu_c \Delta t \gg 1$, the solution is stable but oscillatory as shown in Fig. 1b. Such oscillations would cause unphysical heating of the fluid.

(iii) For $\theta = 1$, which corresponds to an implicit algorithm, Eq. (12) yields

$$u^t = \frac{1}{1+\nu_c \Delta t} u^{t-\Delta t},$$

and for $\nu_c \Delta t \gg 1$, the solution has a stable decay, Fig. 1c, although at a slower rate than the analytic solution.

Returning to the original problem, the velocity at the new time level is obtained by adding the collisional contribution from Eq. (3) to the collisionless velocity given by Eq. (10),

$$u^t_{s,j+1/2} = u^{\text{collisionless}}_{s,j+1/2} - \Delta t \left[\sum_{s'} \frac{m_{ss'}}{m_s} \nu_{ss'} (u^t_s - u^t_{s'}) \right]_{j+1/2}. \quad (13)$$

Note that the collision forces in the right member of Eq. (13) are computed using the velocities at the new time level, u^t_s, corresponding to the stable case $\theta = 1$ in the preceding example. This requires that the set of equations represented by Eq. (13) be solved simultaneously for all species present at the cell boundary $j+1/2$, to obtain the updated velocities from their collisionless values found in Eq. (10),

$$u^t_{s,j+1/2} = [A_{ss'}]^{-1} [u^{\text{collisionless}}_{s',j+1/2}], \quad (14)$$

where

$$A_{ss'} = \begin{bmatrix} 1 + \sum_{s' \neq 1} \Delta t \frac{m_{1s'}}{m_1} \nu_{1s'} & -\Delta t \frac{m_{12}}{m_1} \nu_{12} & \cdots \\ -\Delta t \frac{m_{21}}{m_2} \nu_{21} & 1 + \sum_{s' \neq 2} \Delta t \frac{m_{2s'}}{m_2} \nu_{2s'} & \cdots \\ \cdots & \cdots & \cdots \end{bmatrix} \quad (15)$$

is the collisional momentum coupling matrix at cell boundary $j+1/2$. The time step may now be completed by adding the source term contributions to the momenta,

$$(nu)^t_{s,j} = (nu)^*_{s,j} + \tfrac{1}{2} n^t_{s,j} \times (\Delta u_{s,j+1/2} + \Delta u_{s,j-1/2}), \quad (16)$$

where $\Delta u_{s,j+1/2} = u^t_{s,j+1/2} - u^*_{s,j+1/2}$. For the collisionless case, $\Delta u_{s,j+1/2}$ reduces to the pressure and electric field contributions defined in Eq. (23) of Ref. [1].

For $\nu_c \Delta t \ll 1$, where ν_c is a typical collision frequency, Eq. (14) introduces only a weak collisional coupling between species, which tends to equate their velocities over many time steps. For $\nu_c \Delta t \gg 1$, there is strong collisional coupling between species. Some insight on the behavior of the algorithm in this case may be obtained by considering a single moving species, coupled by collisions to a stationary background. This limiting case approximates electrons colliding with much heavier and less mobile ions. Writing Eq. (14) for the mobile species, $s = 1$, and setting $u_2 = 0$ for the stationary species yields

$$(1 + \nu_{12} \Delta t) u^t_1 = u^*_1 + \Delta t \left[-\frac{1}{m_1 n_1} \frac{\partial}{\partial x} (nT)_1 + \Omega_p \frac{q_1}{m_1} E^t \right] \quad (17)$$

and, for $\nu_{12} \Delta t \gg 1$,

$$u^t_1 \approx \frac{1}{\nu_{12}} \left[-v^2_{\text{th}1} \frac{1}{n_1} \frac{\partial n_1}{\partial x} + \Omega_p \frac{q_1}{m_1} E^t \right]. \quad (18)$$

In Eq. (18), the electric field, velocity, and density gradient are evaluated at cell boundaries, and the fluid has been assumed isothermal, with thermal velocity $v_{\text{th}1} = (T_1/m_1)^{1/2}$.

Consider first the case of a uniform density. The density gradient term in Eq. (18) vanishes and the electric field term gives the correct expression of the mobility in the normalized units considered here, $\Omega_p q_1 / \nu_{12} m_1$. Thus, for large $\nu_{12} \Delta t$, the algorithm automatically gives Ohm's law. Consider now the case of a non-uniform neutral fluid. The electric field term vanishes in this case and substituting u^t_1 from Eq. (18) into the continuity equation, Eq. (1), yields

$$\frac{\partial n_1}{\partial t} = \frac{v^2_{\text{th}1}}{\nu_{12}} \frac{\partial^2 n_1}{\partial x^2} \quad (19)$$

showing that the algorithm automatically reduces to the diffusion model in this limit.

b. *Implicit Electric Field Solution*

The implicit field solution derived in Ref. [1] must be modified to include the effect of collision forces. As in the collisionless case, the starting point is the integral form of the Poisson equation, written at the new time level,

$$E^t_{j+1/2} - E^t_{j-1/2} = \Delta x \, \Omega_p \sum_s q_s n^t_{s,j},$$

and at the old time level,

$$E^0_{j+1/2} - E^0_{j-1/2} = \Delta x \, \Omega_p \sum_s q_s n^0_{s,j}.$$

Subtracting these equations and substituting $n_j^t = n_j^0 - f_{j+1/2} + f_{j-1/2}$, where $f_{j+1/2}$ denotes the fluxes used in the transport algorithm (see Appendix B), yields

$$H^t_{j+1/2} \equiv E^t_{j+1/2} - E^0_{j+1/2} + \Omega_p \, \Delta x \sum_s q_s f_{s,j+1/2} = C^t. \tag{20}$$

Here C^t is a constant, which may be time dependent, but is independent of position. This constant depends on the boundary conditions imposed on the system. For a floating potential, the boundary field is proportional to the surface charge on the wall. Consider the left boundary ($x=0$), where the electric field is $E_{1/2}$. The change in $E_{1/2}$ during one time step, proportional to the flux of charge into the left boundary, is $\Omega_p \, \Delta x \sum q f_{1/2}$. Writing Eq. (20) for $j=0$ shows that C^t must vanish. If the potential across the system is imposed by an external circuit, then C^t is nonzero. The appendix of Ref. [1] considers this case.

The field is solved by applying Newton's iteration method to Eq. (20), writing the new field at iteration level $q+1$ as $E^t \approx E^{q+1} = E^q + \delta E$, where E^q is the new electric field at iteration level q and δE is the correction. All quantities are at cell boundary $j+1/2$ and the subscripts are omitted. Expanding H^{q+1} linearly with respect to δE about the previous iteration gives (for $C^t = 0$)

$$H^{q+1} = H^q + \frac{\partial H^q}{\partial E} \delta E = 0 \tag{21}$$

which can be solved for the correction δE. The differentiation of H^q with respect to E in Eq. (21) must take into account the explicit dependence on E^t in Eq. (20) and the dependence of the flux at cell boundary $j+1/2$ on E through the velocities

$$\frac{\partial H^q}{\partial E} = 1 + \Omega_p \, \Delta x \sum_s q_s \frac{\partial f_s}{\partial E}, \tag{22}$$

where

$$\frac{\partial f_s}{\partial E} = \left(\frac{\partial f}{\partial \varepsilon}\right)_s \frac{\Delta t}{\Delta x} \frac{du_s}{dE} \tag{23}$$

and $\varepsilon_s = u_s \, \Delta t / \Delta x$. The derivative du_s/dE, which takes into account the combined effects of the electric field and collisions, is found from Eqs. (10) and (14),

$$\frac{du_s}{dE} = [A_{ss'}]^{-1} \left[\frac{d}{dE} u_{s'}^{\text{collisionless}}\right] = \Omega_p \, \Delta t \, g_s, \tag{24}$$

where

$$g_s = [A_{ss'}]^{-1} \frac{q_{s'}}{m_{s'}}. \tag{25}$$

Combining Eqs. (22)–(24) to express $\partial H^q / \partial E$, substituting into Eq. (21), and solving for δE yields

$$\delta E = -\frac{E^q - E^0 + \Omega_p \, \Delta x \sum_s q_s f_s^q}{1 + (\Omega_p \, \Delta t)^2 \sum_s q_s \, g_s (\partial f / \partial \varepsilon)_s}. \tag{26}$$

For the case of vanishing collision forces, $g_s = q_s/m_s$, and Eq. (26) reduces to the collisionless results of Ref. [1].

The field solver is implemented in the same way as for the collisionless case [1]. The set of Eqs. (7)–(10), (14)–(16), (25), (26) is iterated. The fluxes f_s and their derivatives $(\partial f/\partial \varepsilon)_s$ depend on the transport algorithm used and the derivatives $(\partial f/\partial \varepsilon)_s$ are approximated by $(f/\varepsilon)_s$ as discussed in Ref. [1]. The iteration loop also includes the temperature equations derived in the next section.

In the computation of the velocities, which require division by density in Eq. (9), vacuum regions corresponding to densities below a floor level, n_{floor}, must be identified. A cell boundary, $j+1/2$, is in the fluid if $n_j, n_{j+1} > n_{\text{floor}}$; it is at a fluid–vacuum interface if $n_j > n_{\text{floor}}$, $n_{j+1} < n_{\text{floor}}$ or $n_j < n_{\text{floor}}$, $n_{j+1} > n_{\text{floor}}$; and it is in a vacuum if n_j, $n_{j+1} < n_{\text{floor}}$. Velocities may be computed from Eq. (9) only for interior boundaries. At a fluid–vacuum interface, the velocity is set equal to the velocity at the adjacent interior boundary. In vacuum regions adjacent to system boundaries, the velocities are also set equal to the value at the last non-vacuum cell boundary. This guarantees that fluid with density below the floor, which corresponds to the vacuum, will flow ahead of the fluid. In vacuum regions which are sandwiched between two fluid regions, the velocities are linearly interpolated to minimize the velocity gradient. In this case, pile-up of fluid below the floor level is possible, but is minimized.

The transport algorithm requires that the time step, Δt, satisfy the Courant condition, $u_{\max} \, \Delta t / \Delta x < 1$, where $u_{\max}$ denotes the maximum velocity of any species. This condition implies other limitations on the time step, which can be derived from Eq. (17), where species 1 is the most mobile fluid component, generally electrons.

A first condition is derived from the pressure term in the bracket in the right member of Eq. (17). Assuming an isothermal fluid, this term may be written as $v_{\text{th1}}^2 (\partial n_1/\partial x)/n_1$. Since the mesh size, Δx, is the shortest possible scale length, the maximum velocity which can be generated by this term is

$$u_{\max} = \frac{\Delta t}{1 + \nu_{12} \, \Delta t} \frac{v_{\text{th1}}^2}{\Delta x}. \tag{27}$$

Substituting this value of u_{max} in the Courant condition, $u_{max}\,\Delta t/\Delta x < 1$ yields

$$\frac{v_{th1}^2}{1+\nu_{12}\,\Delta t}\frac{\Delta t^2}{\Delta x^2} < 1. \tag{28}$$

For weak collisions, $\nu_{12}\,\Delta t \ll 1$, Eq. (28) reduces to $v_{th1}\,\Delta t/\Delta x < 1$, which is the familiar Courant condition on the sound speed. For strong collisions, $\nu_{12}\,\Delta t \gg 1$, Eq. (28) reduces to $(v_{th1}^2/\nu_{12})\,\Delta t/\Delta x^2 < 1$. This guarantees that the Neumann stability condition for the diffusion model described by Eq. (19), is automatically satisfied.

A second condition is derived from the electric field term in the right member of Eq. (17). The maximum velocity which can be built up from this term in a single time step is

$$u_{max} = \frac{\Delta t\,\Omega_p}{1+\nu_{12}\,\Delta t}\frac{q_1}{m_1}E.$$

Substituting this value of u_{max} in the Courant condition $u_{max}\,\Delta t/\Delta x < 1$ yields

$$\frac{\Omega_p q_1 E}{m_1\,\Delta x}\frac{\Delta t^2}{1+\nu_{12}\,\Delta t} < 1. \tag{29}$$

For weak collisions, $\nu_{12}\,\Delta t \ll 1$, condition (29) may be written in the form $\omega_T\,\Delta t < 1$, where $\omega_T = (\Omega_p q_1 E/m_1\,\Delta x)^{1/2}$ is the maximum trapping frequency corresponding to a particle in an electric field of amplitude E and scale length Δx. This condition is familiar in implicit particle simulations and still applies in the present simulations, even though the fluid formulation adopted here is not capable of representing trapping oscillations. For strong collisions, $\nu_{12}\,\Delta t \gg 1$, Eq. (29) yields $(\Omega_p q_1 E/m_1\nu_{12})\,\Delta t/\Delta x < 1$. In this limit, the condition simply reduces to the Courant condition on the drift velocity, $u_{drift} = \Omega_p q_1 E/m_1\nu_{12}$.

III. ENERGY EQUATIONS

Solution of the energy equations involves updating the temperatures with the source terms given by Eq. (6) and transporting the internal energy according to Eq. (5). To ensure a stable solution for large values of $\nu_{ss'}\,\Delta t$, the temperature source terms are applied in three substeps, corresponding to (i) the work of pressure forces and dissipation, (ii) temperature equilibration, and (iii) heat conduction.

Starting from the old temperatures, $T_{s,j}^{(0)}$, for each species s, partially updated temperatures, $T_{s,j}^{(1)}$, are computed using the first two terms of Eq. (6),

$$T_{s,j}^{(1)} = T_{s,j}^{(0)} - \frac{2}{3}\frac{\Delta t}{\Delta x}\frac{P_{s,j}^{(0)}}{n_{s,j}^{(0)}}\left[u_{j+1/2} - u_{j-1/2}\right]_s^t + \frac{1}{2}\left[\delta T_{j+1/2} + \delta T_{j-1/2}\right]_s, \tag{30}$$

where

$$\delta T_{s,j+1/2} = \frac{2}{3}\Delta t \sum_{s'}\frac{m_{ss'}^2}{m_s}\left[\nu_{ss'}(u_s - u_{s'})^2\right]_{j+1/2}^t \tag{3}$$

are temperature increments at cell boundaries, which a averaged and added to the cell-centered temperatures. Nc that Eq. (30) can yield only positive values of the te peratures $T_{s,j}^{(1)}$, as long as the old temperatures, $T_{s,j}^{(0)}$, themselves positive and the velocities satisfy the Coura condition, $u\,\Delta t/\Delta x < 1$. The same values of the collisi frequencies at cell boundaries are used in Eq. (31) as in t momentum coupling matrix, Eq. (15).

Temperature equilibration between species is done solving the set of equations,

$$\frac{3}{2}\frac{dT_s}{dt} = -\sum_{s'\neq s} B_{ss'}n_{s'}(T_s - T_{s'}) \tag{3}$$

for each cell. Since equilibration between species can cau large temperature changes in a single time step, Eq. (3 needs to be solved analytically over the time interval Δ This is done by the standard diagonalization method. T quantities $B_{ss'}$, which are defined in Section I, a symmetric, but the temperature coefficients $B_{ss'}n_{s'}$ are n symmetric and the set of equations represented by Eq. (3 has to be symmetrized prior to diagonalization. L $T_s' = T_s(n_s)^{1/2}$, then Eq. (32) yields

$$\frac{3}{2}\frac{dT_s'}{dt} = \sum_{s'\neq s} B_{ss'}\sqrt{n_s n_{s'}}\,T_{s'}' - \left[\sum_{s'\neq s} B_{ss'}n_{s'}\right]T_s'$$

or, in matrix form,

$$\frac{d}{dt}[T'] + \frac{2}{3}S[T'] = 0,$$

where $[T']$ denotes a column vector of the temperatur and

$$S = \begin{bmatrix} B_{12}n_2 + B_{13}n_3 + \cdots & -B_{12}\sqrt{n_1 n_2} & \cdots \\ -B_{21}\sqrt{n_2 n_1} & B_{21}n_1 + B_{23}n_3 + \cdots & \cdots \\ & \cdots & \end{bmatrix} \tag{3}$$

is symmetric. Diagonalization gives real eigenvalues, σ and orthonormal eigenvectors $[b]_s$. Using these eige vectors to form the columns of a matrix with elements b_s the equilibrated temperatures are computed,

$$T_s^{(2)} = \frac{1}{\sqrt{n_s}}\sum_{s',s''} b_{ss'}b_{s''s'}\sqrt{n_{s''}}\,T_{s''}^{(1)}\exp\left[-\frac{2}{3}\sigma_{s'}\,\Delta t\right]. \tag{3}$$

Heat conduction is computed in a third substep by solving the diffusion equation,

$$\frac{3}{2} n \frac{\partial T}{\partial t} = \frac{\partial}{\partial x} \kappa \frac{\partial T}{\partial x},$$

separately for each species. The heat conduction coefficient, κ, is proportional to the local density and depends on the temperature as discussed in Appendix A. This equation is solved by a simple implicit scheme,

$$D_j^+ T_{j+1}^{(3)} + D_j^0 T_j^{(3)} + D_j^- T_{j-1}^{(3)} = \tfrac{3}{2} n_j T_j^{(2)}. \tag{35}$$

Here, $T_j^{(3)}$ is the partially updated temperature after heat conduction,

$$\begin{aligned} D_j^{\pm} &= -\frac{\Delta t}{\Delta x^2} \kappa_{j \pm 1/2} \\ D_j^0 &= \tfrac{3}{2} n_j - D_j^+ - D_j^- \end{aligned} \tag{36}$$

and $\kappa_{j+1/2} \propto (n_j + n_{j+1})/2$ denotes the heat conductivity at the cell boundaries. This scheme is stable for arbitrary time steps and requires only the solution of a tridiagonal system of equations. However, for a vacuum cell which is surrounded by two other vacuum cells, such as cells $j = 5$ or 6 in Fig. 2a, all the terms of Eq. (35) vanish, causing the matrix to become singular. Such singularities could be removed by identifying fluid regions and solving the heat conduction problem separately within each region, with zero-flux conditions at the vacuum boundaries. An equivalent and simpler method is to reset $D_j^{\pm} = 1$, $D_j^0 = -2$, for the values of j where all the coefficients of Eq. (35) vanish, and to proceed with the tridiagonal solution over the entire system. At fluid–vacuum boundaries, such as cell $j = 4$ (or $j = 7$) in Fig. 2a, $n_j = n_{j+1} = 0$ (or $n_j = n_{j-1} = 0$). It follows that $\kappa_{j+1/2} = 0$ (or $\kappa_{j-1/2} = 0$) and substitution into Eq. (36) gives $D_j^+ = 0$ and $D_j^0 = -D_j^-$ (or $D_j^- = 0$ and $D_j^0 = -D_j^+$). Substituting these values into Eq. (35) yields $T_j^{(3)} = T_{j-1}^{(3)}$ (or $T_j^{(3)} = T_{j+1}^{(3)}$), so that the zero heat flux boundary conditions are automatically satisfied. Within the vacuum regions, Eq. (35) takes the form $T_{j+1}^{(3)} - 2T_j^{(3)} + T_{j-1}^{(3)} = 0$, giving a linear interpolation of the values of the temperature in these regions, as shown in Fig. 2b.

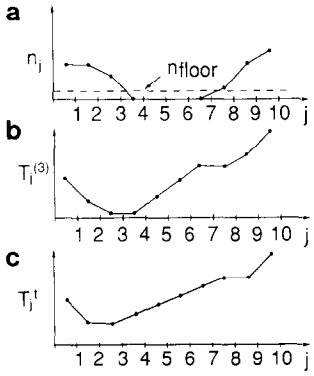

FIG. 2. Heat conduction algorithm including a vacuum region. (a) Density showing vacuum cells. (b) Temperature resulting from reseting $D_j^{\pm} = 1$ and $D_j^0 = -2$ in vacuum cells surrounded by two other vacuum cells. (c) Effect of resetting the temperature at the boundary cells.

After application of the temperature source terms, the energy is transported as was done in Ref. [1] for the collisionless case to obtain the updated temperature,

$$T_j^t = \frac{1}{n_j^t} \Psi[n_j^0 T_j^{(3)}, u_{j+1/2}^t]. \tag{37}$$

Temperature may be computed from Eq. (37) for fluid cells, where the density is above the floor level, $n_j^t > n_{\text{floor}}$. However, the temperature source contributions from Eq. (6) are inaccurate in cells which are adjacent to vacuum, such as $j = 3$ and $j = 8$ in Fig. 2b, because they involve velocities at vacuum boundaries, which are artificially set in the solution of the momentum equations. Therefore, temperature is computed from Eq. (37) only in fluid cells, which are surrounded by two other fluid cells. In cells which are adjacent to vacuum, such as $j = 3$ and $j = 8$ in Fig. 2, the temperature is set equal to the adjacent interior cell, $j = 2$ and $j = 9$ in Fig. 2c.

The computation of the temperatures from Eqs. (30), (34), (35), (37) is included in the same iteration loop as the computations of the density, momentum, and electric field described in Section II. The velocities used to compute dissipation in Eq. (31) must be the velocities most recently updated from Eq. (14) to guarantee that dissipation scales as $(v_{ss'})^{-1}$. This prevents unphysical heating at the interface between adjacent fluids.

IV. NUMERICAL TESTS

A code implementing the algorithms of Sections II and III has been written and numerical tests involving collisional coupling between neutral fluids or plasmas are presented in this section.

a. *Ohmic Heating*

An electric field is applied to a uniform plasma consisting of electrons interacting with stationary ions by Coulomb collisions with collision frequency $\nu_{ei} = \nu_0 (T_e/T_0)^{-3/2}$, where T_0 and ν_0 are the initial temperature and collision frequency. An analytic solution of this problem is derived

first. The electron momentum and energy equations reduce to

$$\frac{du_e}{dt} = -\frac{eE}{m_e} - \nu_{ei} u_e \tag{38}$$

$$\frac{dT_e}{dt} = \frac{2}{3} m_e \nu_{ei} u_e^2. \tag{39}$$

For sufficiently small electric fields, to be determined a posteriori, the acceleration term in the left member of Eq. (38) may be neglected, whence $u_e = -eE/m_e\nu_{ei}$. Substituting this expression into Eq. (39), gives

$$\frac{d}{dt}\left(\frac{T_e}{T_0}\right) = 2\alpha\left(\frac{T_e}{T_0}\right)^{3/2},$$

where $\alpha = e^2E^2/3m_e\nu_0 T_0$. Solving this equation yields

$$T_e = T_0(1-\alpha t)^{-2},$$

where $u_0 = -eE/m_e\nu_0$ is the initial drift velocity. From Eqs. (40), the runaway time is α^{-1} and the solution is valid only for $\alpha t \ll 1$. The condition under which the acceleration term in Eq. (38) can be neglected may now be found. From the first of Eqs. (40),

$$\frac{du_e}{dt} = \frac{3\alpha u_e}{1-\alpha t} \ll \frac{eE}{m_e}$$

or

$$\frac{u_e}{u_0} \ll \frac{\nu_0(1-\alpha t)}{3\alpha}. \tag{41}$$

A computer simulation was done with an electric field and initial collision frequency such that $\nu_0 t_0 = 133$. Here, $t_0 = m_e\nu_0/eE$ is the normalization time, corresponding to the time needed to accelerate a collisionless electron to the thermal velocity, $v_0 = (T_0/m_e)^{1/2}$. It follows that $\alpha t_0 = (3\nu_0 t_0)^{-1} = 2.5\times10^{-3}$, giving a runaway time $\alpha^{-1} = 400t_0$ and an initial drift velocity $u_0 = v_0/\nu_0 t_0 = 7.5\times10^{-3}v_0$. The simulation was done with a density corresponding to $\omega_{pe}t_0 = 10^3$ and $\Delta t = 0.1t_0$ ($\omega_{pe}\Delta t = 100$). The result is shown in Fig. 3, where the solid line corresponds to the simulation and the points are analytical values from Eq. (40). The initial rise from zero to 7.5×10^{-3} corresponds to the initial rise of the applied electric field. The computation was stopped at $t_{max} = 100t_0$, well before runaway time ($\alpha t_{max} = 0.25$) and at this time, condition (41) is satisfied,

$$\frac{u_{max}}{u_0} = 2.4 \ll \frac{\nu_0(1-\alpha t_{max})}{3\alpha} = 1.33\times10^4.$$

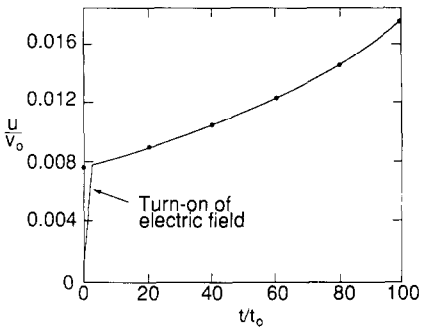

FIG. 3. Drift velocity vs. time for the ohmic heating test with Coulomb collisions. Simulation results are shown in solid line and the points denote analytical results.

b. *Friction Tests*

In the present algorithms, the contact force at the interface between adjacent fluids is transmitted by friction forces. In the case of a short mean free path, this region can be small, extending over only a few cells. To examine the performance of the algorithms in this regime, the present tests consider a shock problem in which two neutral fluids consisting of identical species overlap over two cells at an initial density discontinuity of 10 to 1 at $x = 50\,\Delta x$, corresponding to the center of the system. These simulations include friction, dissipation, and temperature equilibration, but exclude heat conduction. The collision frequency between fluids is

$$\nu_{ss'} = \nu_0 \frac{n_{s'}}{n_0}\sqrt{(T_s + T_{s'})/T_0},$$

where n_0 is the upper density and T_0 is the initial temperature of both fluids. This temperature dependence of the collision frequency corresponds to the hard sphere collision model. The transport scheme in these simulations used the "min-mod" limiter described in Appendix B.

A first simulation was done with $\nu_0 t_0 = 5\times10^3$, where $t_0 = \Delta x/v_0$ is used as normalization time, $v_0 = (T_0/m_0)^{1/2}$ is the normalization velocity and $m_0 = m_1 = m_2$. Thus, the mean free path is $\lambda_{21} = (\nu_0 t_0)^{-1}\,\Delta x = 2\times10^{-4}\,\Delta x$ in the upper density region and $\lambda_{12} = 2\times10^{-3}\,\Delta x$ in the lower density region, very small fractions of the mesh size, so that both fluids are strongly collisional. The time step is $\Delta t = 0.1t_0$. The total density, $n_{tot} = n_1 + n_2$, mean velocity, $u_{av} = (n_1u_1 + n_2u_2)/n_{tot}$, and mean temperature, $T_{av} = (n_1T_1 + n_2T_2)/n_{tot}$ after 200 time steps are plotted in Fig. 4 (solid lines). The total fluid displays the expected shock structure, with an expansion region from 25 to 50 Δx, a contact discontinuity at $\approx 67\,\Delta x$, and a shock front at $\approx 90\,\Delta x$. These results are not distinguishable from the results of a simulation with a single fluid. This demonstrates that the two fluids push upon each other in their contact

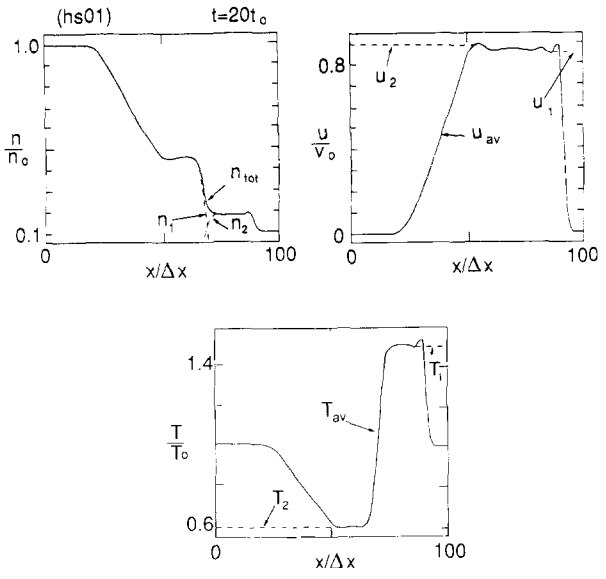

FIG. 4. Simulation results for a shock wave problem initialized with a neutral fluid artificially divided into two identical fluids in contact at a density discontinuity of 10 to 1. The normalized collision frequency is $\nu_0 t_0 = 5 \times 10^3$. Densities, n, velocities, u, and temperatures, T, are shown at $t = 20t_0$. Values corresponding to the total fluid $n_{tot} = n_1 + n_2$, $u_{av} = (n_1 u_1 + n_2 u_2)/n_{tot}$, and $T_{av} = (n_1 T_1 + n_2 T_2)/n_{tot}$ are shown in solid lines and values for the individual fluids are shown in broken lines.

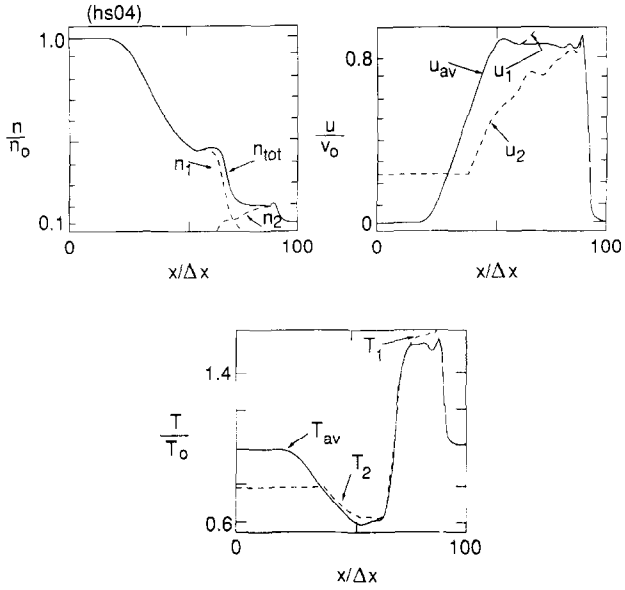

FIG. 5. Simulation results for the same problem as in Fig. 4, but for a normalized collision frequency $\nu_0 t_0 = 5$.

region without generating unphysical effects. The densities, velocities, and temperatures of the individual fluids are also plotted in Fig. 4 (broken lines). Note that the two fluids continue to meet at the contact discontinuity, that their velocities are very close in the contact region, and that there is no significant heating due to friction. Logarithmic plots of the densities, not shown here, indicate that there is mixing between the fluids over a significant region, but with partial densities that are several orders of magnitude below the total density.

A second simulation was done with smaller collision frequencies corresponding to $\nu_0 t_0 = 5$, giving mean free paths $\lambda_{21} = 0.2\,\Delta x$ and $\lambda_{12} = 2\,\Delta x$. The total density and the mean velocity and temperature, plotted in Fig. 5 do not show a significant difference compared to the strong collision case of Fig. 4, but there is now more mixing between the fluids. The individual velocities of the two fluids are also significantly different. This simulation was done with $\Delta t = 0.025 t_0$ to satisfy the Courant condition on u_1 which becomes large in the low density region to the right of the system.

c. *Colliding Plasmas*

Consider two hot plasma slabs adjacent to one another. Initially their electron and ion densities have identical trapezoidal profiles as shown in Fig. 6, with a distance $d = 110\,\Delta x$ between centers. As in the previous example, time will be normalized to $t_0 = \Delta x / v_0$, where $v_0 = (T_0/m_e)^{1/2}$ is the normalization velocity and T_0 is the normalization temperature. These slabs could represent laser-heated exploding foils; assuming $\Delta x = 1\ \mu$m, each foil would have a full width at half maximum of $20\ \mu$m and the distance between centers would be $110\ \mu$m.

A preliminary simulation was done with a single neutral fluid (no electric field). The particle mass was set to $m = 100\, m_0$ and the temperature to $T = 1.1 T_0$ to correspond to the plasma case to be treated with multiple fluids. The time step for this simulation was $\Delta t = 0.5 t_0$. At $t = 240 t_0$, the slabs have expanded into each other and the leading edges of their expansions have come into contact at the center of the system and stagnated. This results in recompression of the fluid on both sides of the center, and a high-temperature spike, $T = 12.5 T_0$ at the center as shown in Fig. 7. At $t = 600 t_0$, more fluid from the expanding slabs moves inward and stagnates, resulting in symmetric outward moving shocks. At this time the central region also decompresses and the temperature profile broadens, see Fig. 7.

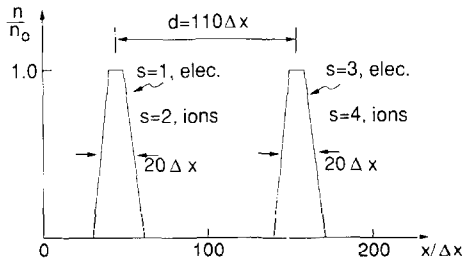

FIG. 6. Density initialization of colliding plasma slabs.

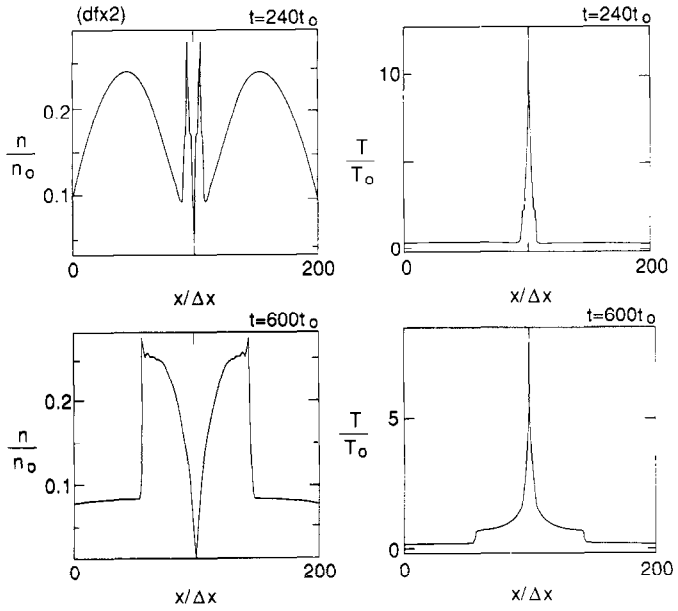

FIG. 7. Densities and temperatures at $t = 240t_0$ and $t = 600t_0$ from a simulation of colliding plasma slabs using a single neutral fluid.

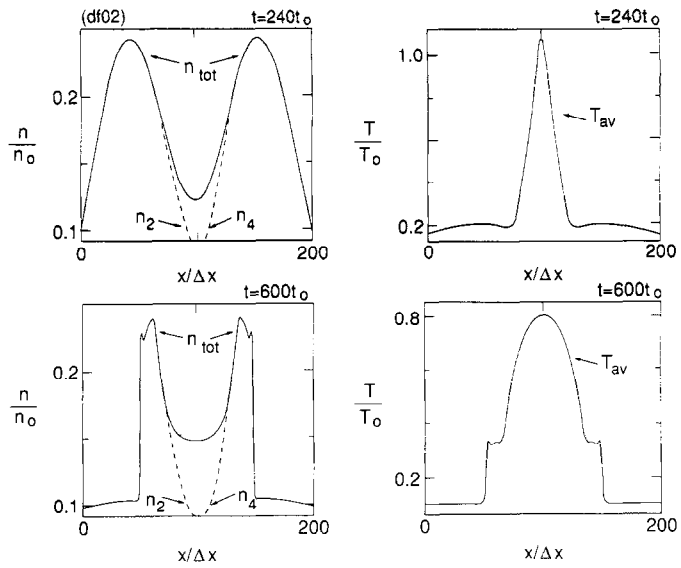

FIG. 8. Densities and ion temperatures at $t = 240t_0$ and $t = 600t_0$ from a simulation of colliding plasma slabs using multiple fluids, with collision parameter $\eta = 6.8 \times 10^{-3}$. Values corresponding to the total ion fluid, $n_{tot} = n_2 + n_4$ and $T_{av} = (n_2 T_2 + n_4 T_4)/n_{tot}$ are shown in solid line and values for individual ion fluids are shown in broken line.

In the multifluid simulations, the plasma slabs are initialized using four fluids, $s = 1$ (and 2) for the electrons (and ions) in the left slab and $s = 3$ (and 4) for the electrons (and ions) to the right. This allows the fluids to stream through each other when the plasma slabs collide after expanding. Initially the electron and ion temperatures are $T_e = T_0$, $T_i = 0.1T_0$ and the simulations include friction, dissipation, temperature equilibration, and heat conduction with a flux limiter set to 0.3 (see Appendix A for the definition of the flux limiter). For the purpose of this numerical test, an artificial mass ratio $m_i/m_e = 100$ is chosen. The initial density is such that $\omega_p t_0 = 10^3$; the time step is $\Delta t = 0.2t_0$ giving $\omega_p \Delta t = 200$. The collisionality is specified by the dimensionless parameter

$$\eta = 3\sqrt{\pi/2} \Big/ \left(\frac{d}{\Delta x}\right) (\omega_p t_0)^2 \left(\frac{e^2}{T_0 \Delta x}\right) \Lambda,$$

where Λ is the Coulomb logarithm, Δx is chosen as normalization length, $t_0 = \Delta x/v_0$ is the normalization time, and $v_0 = (T_0/m_0)^{1/2}$ is the normalization velocity. This parameter is approximately the ratio of the mean-free-path $\lambda_{ii} = (T_0/m_i)^{1/2}/\nu_{ii}$, to the scale length d, $\eta \approx \lambda_{ii}/d$. In terms of η, Eq. (A5) gives the collision frequencies for singly ionized ions as

$$\nu_{ss'} = \frac{1}{\eta d} \frac{n_{s'}}{m_{ss'}^{1/2} T_{ss'}^{3/2}},$$

where all quantities are normalized. The collision frequencies as defined here do not take into account the relative streaming velocity between species. This velocity dependence is not important for our present purpose of testing the algorithms; however, simulations which include this dependence have been made for realistic parameters [6].

The first simulation was done with $\eta = 6.8 \times 10^{-3}$. In contrast to the single fluid case, the fluids at $t = 240t_0$ do not stagnate abruptly, but stream relative to each other as they come into contact at the center of the system. There is superposition of the fluids in the center of the system with some recompression, but the ion temperature spike is now only $T_{av} = 1.1T_0$, see Fig. 8. At time $t = 600t_0$, outward moving shocks have developed as in the single-fluid case. However, the fluid in the central region behind these shocks is cooler and more uniform.

Two additional multi-fluid simulations were done with collision parameters, η, one order of magnitude lower and

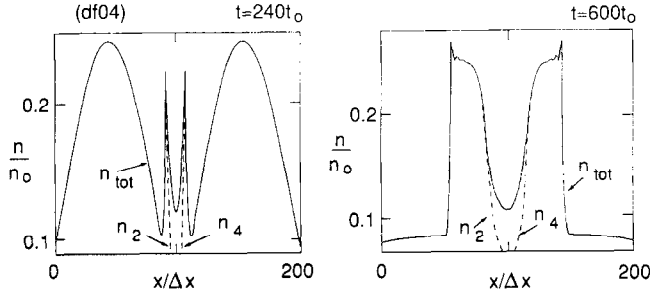

FIG. 9. Densities at $t = 240t_0$ and $t = 600t_0$ from a simulation of colliding plasma slabs using multiple fluids, with $\eta = 6.8 \times 10^{-4}$ corresponding to a higher collisionality than for the case of Fig. 8.

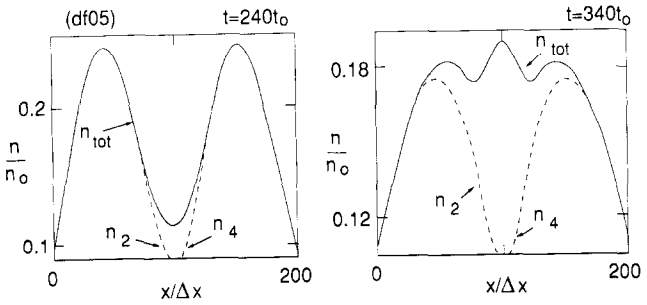

FIG. 10. Densities at $t = 240t_0$ and $t = 340t_0$ from a simulation of colliding plasma slabs using multiple fluids, with $\eta = 6.8 \times 10^{-2}$ corresponding to a lower collisionality than for the case of Fig. 8.

higher than in the case of Fig. 8. For $\eta = 6.8 \times 10^{-4}$ (higher collisionality), the density profiles at $t = 240t_0$ and at $t = 600t_0$, shown in Fig. 9, are similar to the single fluid case, Fig. 7. For $\eta = 6.8 \times 10^{-2}$ (lower collisionality), the density profiles at $t = 240t_0$ and at $t = 340t_0$ simply show a superposition of the slab expansions, see Fig. 10.

d. *Plasma Shocks*

In the following tests, two fluids are used to represent electrons and ions in plasma shock problems. These fluids are initialized such that the plasma is neutral, $n_e = n_i$ and $u_e = u_i$, and with density and temperature discontinuities at $x = 70\,\Delta x$ in a system of length $100\,\Delta x$. A mass ratio $m_i/m_e = 200$ is assumed, the plasma frequency at the reference density n_0 is $\omega_{p0} = 10^3 t_0^{-1}$, $t_0 = \Delta x/v_0$ is the normalization time, $v_0 = (T_0/m_e)^{1/2}$, and T_0 is the normalization temperature. The ratio of specific heats is $\gamma = 5/3$ for both electrons and ions. Except as noted, the time step for these simulations is $\Delta t = 0.4t_0$ and the artificial viscosity is set to $\kappa = 2$.

A simulation excluding collisional effects (friction, dissipation, temperature equilibration) and heat conduction is presented first, after which simulation results including these effects will be discussed. For the large value of $\omega_p t_0$ considered here, the plasma remains quasi-neutral and in the absence of collisions and heat conduction, the plasma shock (with singly ionized ions) should develop as for a neutral fluid, with density $n = n_e = n_i$, velocity $u = u_e = u_i$, and temperature $T = T_e + T_i$, obeying the Rankine Hugoniot relations [7]. Denoting the upstream quantities, to the right of the discontinuity, with subscript 1, and the downstream quantities with subscript 2, the initial values are set by choosing $n_1 = 0.1n_0$, $T_{e1} = T_{i1} = T_1/2 = 0.05T_0$, and $n_2 = 0.335n_0$. The Rankine–Hugoniot relations for a steady shock then give the pressure ratio $p_2/p_1 = 19$ and $T_2 = T_{e2} + T_{i2} = 0.567T_0$. The upstream and downstream sound speeds are $c_1 = (\gamma T_1/m_i)^{1/2} = 0.029v_0$ and $c_2 = 0.069v_0$, from which $u_1 = -0.114v_0$ and $u_2 = -0.034v_0$. In the absence of collisions and heat conduction, the electrons move adiabatically across the shock [8], $T_{e2}/T_{e1} = (n_2/n_1)^{2/3}$, from which, $T_{e2} = 0.112T_0$ and $T_{i2} = T_2 - T_{e2} = 0.45T_0$. These values are listed as the theoretical values in Table I. After a transient, during which the shock acquires a finite thickness and a perturbation travels downstream and disappears into the left boundary, a steady state is reached and, at $t = 3200t_0$, the simulation values listed in Table I are obtained. The electron and ion temperature profiles are also plotted as broken lines in Fig. 11. There is good agreement between theory and simulation, except for the electron temperature which has an 8% error. This agreement was also found to depend on choosing an artificial viscosity coefficient $\kappa \geqslant 2$.

TABLE I

Downstream Steady-State Values for Collisionless Plasma Shock Simulations with $n_1 = 0.1$, $u_1 = -0.114$, $T_{e1} = T_{i1} = 0.05$

	Theory	Simulation
n_2	0.335	0.335
u_2	−0.034	−0.034
T_{e2}	0.112	0.122
T_{i2}	0.45	0.45
$\phi_2 - \phi_1$	1.55×10^{-4}	1.65×10^{-4}

Note. All quantities are normalized.

With $\omega_p t_0 \gg 1$, the electric field is ambipolar,

$$\frac{d\varphi}{dx} = \frac{1}{\omega_{p0} t_0} \frac{1}{n_e} \frac{d}{dx}(n_e T_e),$$

where φ is the electric potential. Since the electrons are adiabatic, T_e may be related to n_e, allowing this equation to be integrated across the shock, from which,

$$\varphi_2 - \varphi_1 = \frac{5}{2} \frac{T_{e1}}{\omega_{p0} t_0} [(n_2/n_1)^{2/3} - 1]$$
$$= 1.55 \times 10^{-4} E_0\, \Delta x,$$

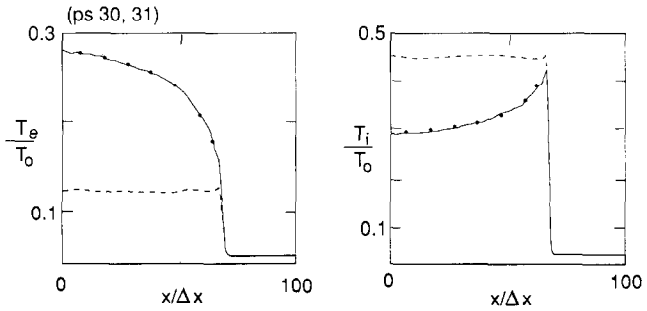

FIG. 11. Electron and ion temperatures for plasma shock. Broken lines correspond to the collisionless simulation, solid lines correspond to a collisional simulation with $e^2/(T_0\,\Delta x) = 2 \times 10^{-8}$ and a Coulomb logarithm $\Lambda = 5$, excluding heat conduction. The points correspond to theoretical values.

where $E_0 = (4\pi n_0 T_0)^{1/2}$ is the electric field normalization, see Section I. This value may be compared with the simulation value, $\phi_2 - \phi_1 = 1.65 \times 10^{-4} E_0 \Delta x$.

A simulation including collisional effects, but excluding heat conduction, is considered next. This would occur in the presence of a magnetic field parallel to the shock front, inhibiting heat conduction, and this case has been studied by Shafranov [9]. Since the plasma remains quasi-neutral, $u_e = u_i$, there is no dissipation and the new effects are limited to temperature equilibration between species, downstream from the shock front. This temperature equilibration does not affect the sum of the electron and ion temperatures, $T_2 = T_{e2} + T_{i2}$, which remains constant. Whence, the density and velocity downstream from the shock are unchanged from the collisionless case and remain constant. Under these conditions, the electron energy equation, obtained from Eqs. (5) and (6), reduces to

$$\frac{3}{2} u_2 \frac{dT_e}{dx} = -B_{ei} n_2 (T_e - T_i). \tag{42}$$

Since $m_i = 200 m_e \gg m_e$, $B_{ei} = 3(m_e/m_i) C_{ei}$, where $C_{ei} = C_0/T_e^{3/2}$ and the constant C_0 which depends on the collisionality, may be computed from Eq. (A5). For $\omega_{p0} t_0 = 10^3$, a collisionality specified by $e^2/(T_0 \Delta x) = 2 \times 10^{-8}$ and $\Lambda = 5$, Eq. (A5) gives $C_0 = 2.66 \times 10^{-2}$. Defining $T^* = T_2/2 = \text{const}$ and $\beta = \frac{4}{3} B_{ei}(T^*) n_2/u_2$, Eq. (42) reduces to

$$\frac{d}{dx}\frac{T_e}{T^*} = -\beta \left[\frac{T_e}{T^*}\right]^{-3/2} \left[\frac{T_e}{T^*} - 1\right]. \tag{43}$$

This equation is solved, giving

$$T_e = T^* \Phi^{-1}\left[\Phi\left[\frac{T_{e2}}{T^*}\right] - \beta x\right],$$
$$T_i = 2T^* - T_e, \tag{44}$$

where T_{e2} is the electron temperature immediately downstream of the shock, x is the distance downstream of the shock, and

$$\Phi(\xi) = 2\sqrt{\xi} + \frac{2}{3}\xi^{3/2} - \ln\left[\frac{1+\sqrt{\xi}}{1-\sqrt{\xi}}\right]. \tag{45}$$

These results are identical to Eq. (15) of Ref. [9].

The simulation is initialized as in the collisionless case and the electron and ion temperatures at $t = 3200 t_0$ are plotted in solid lines in Fig. 11. Note that the temperatures equilibrate downstream from the shock and approach the equilibrium value $T^* = 0.285 T_0$. The theoretical values from Eqs. (44) and (45), with $T_{e2} = 0.112 T_0$ and $T^* = 0.285 T_0$, are plotted as points in Fig. 11, showing good agreement between theory and simulation.

Finally, a simulation including both collisions and heat conduction is considered. Heat conduction affects the electrons directly, heating them upstream of the shock and causing their temperature to become continuous across the shock [8, 9]. The ion temperature remains discontinuous across the shock, but is modified upstream of the shock by equilibration with the electrons. Downstream of the shock, there is also equilibration between electron and ion temperatures as in the preceding case, and the Rankine–Hugoniot relations are satisfied between region 1, far upstream of the shock, and region 2, far downstream of the shock. The simulation is initialized as in the preceding case, with upstream and downstream values of n, u, T_e, and T_i given in Table I. The collisionality is specified by setting $e^2/(T_0 \Delta x) = 2 \times 10^{-8}$ and $\Lambda = 5$, and the thermal conductivity is computed without flux limiting. A longer system, $150\,\Delta x$, is used with the discontinuity at $x = 120\,\Delta x$, to allow more space for heat conduction and temperature equilibration behind the shock. The electron and ion temperature profiles at $t = 6000 t_0$ are plotted in Fig. 12. The values of n, u, and T_i immediately upstream and downstream of the shock, denoted by subscripts 01 and 02, are listed in Table II. The electron temperature is indeed continuous across the shock and there are continuous changes in all quantities both upstream and downstream.

The theory of this shock phenomenon was developed by Shafranov [9]. The electron and ion energy equations yield

$$\frac{dT_e}{dx} = J\kappa_e^{-1}\left[\frac{5}{2}(T - T_1) + \frac{1}{2} m_i (u^2 - u_1^2)\right]$$
$$\frac{dT_i}{dx} = \left(1 \Big/ \left(\frac{3}{2} - \frac{T_i}{m_i u^2 - T}\right)\right) \tag{46}$$
$$\times \left[\frac{T_i}{m_i u^2 - T}\frac{dT_e}{dx} + 3C_{ei}\frac{m_e}{m_i}\frac{J}{u^2}(T_e - T_i)\right],$$

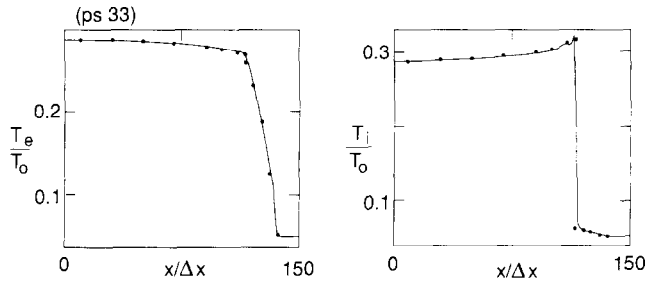

FIG. 12. Electron and ion temperatures for a collisional plasma shock with the same collisional parameters as in Fig. 11, but including heat conduction. The solid lines correspond to the simulations and the points were computed from Shafranov's theory [9].

where $J = nu = \text{const.}$ and $T = T_e + T_i$. These equations apply both upstream and downstream of the shock discontinuity, the ion heat conduction has been neglected, and the electron heat conductivity is evaluated without flux limiting, $\kappa_e^{-1} = (1+\sqrt{2})\, C_0 T_e^{-5/2}$. Mass and momentum conservation determines the local velocity as a function of the sum of the temperatures T,

$$u = \frac{1}{2} u_1 \left[1 + \frac{T_1}{m_i u_1^2}\right] \times \left[1 \pm \sqrt{1 - \frac{4T/m_i u_1^2}{[1 + T_1/m_i u_1^2]^2}}\right], \tag{47}$$

where the positive sign applies to the upstream (supersonic) side and the negative sign applies to the downstream (subsonic) side.

The jump conditions for the velocity and for the ion temperature across the shock discontinuity are

$$\frac{u_{02}}{u_{01}} = \frac{1}{4} + \frac{5}{4}\frac{T_1}{m_i u_1^2} - \frac{T_{e0}}{2m_i u_1^2}\frac{1}{u_{02}/u_{01} - 1} \ln \frac{u_{02}}{u_{01}} \tag{48}$$

and

$$\frac{5}{2}(T_{i02} - T_{i01}) + \frac{1}{2} m_i (u_{02}^2 - u_{01}^2) - T_{e0} \ln \frac{u_{02}}{u_{01}} = 0. \tag{49}$$

Recall that the subscripts "01" and "02" denote conditions immediately upstream and downstream of the shock and that T_{e0} is the electron temperature at the shock, which is continuous. Note that Eqs. (48) and (49) are similar to the classical shock equations, except for the logarithmic terms, which account for the acceleration and the work done on the fluid due to the ambipolar field across the shock. The u_1, and $T_{e1} = T_{i1}$ far ahead of the shock. The values far downstream, n_2, u_2, and $T_{e2} = T_{i2}$ are determined from the Rankine–Hugoniot relations, taking $T = T_e + T_i$. If the electron temperature T_{e0} at the shock and the ion temperature T_{i01} immediately ahead of the shock were specified, Eqs. (47)–(49) would allow determination of the remaining quantities, u_{01}, u_{02}, and T_{i02}. These values could then be used as boundary values to solve the differential equations, Eqs. (46) in the upstream and downstream regions. However, these solutions must be continuous out to $x = \pm\infty$, where they must approach temperature equilibration, and this occurs only for the proper choice of T_{e0} and T_{i01}. Therefore the theoretical solution of the present shock problem is reached by a series of trials in which T_{e0} and T_{i01} are varied until the desired behavior of T_e and T_i as a function of x is obtained. Results of this theoretical solution are plotted as points in Fig. 12 and are listed in Table II. Both Fig. 12 and Table II show good agreement between simulation and theoretical results.

TABLE II

Values Immediately Upstream and Downstream of Plasma Shock for Collisional Simulation (with Heat Conduction) with $n_1 = 0.1$, $u_1 = -0.114$, $T_{e1} = T_{i1} = 0.05$

	Theory	Simulation
n_{01}	0.111	0.11
n_{02}	0.326	0.33
u_{01}	−0.102	−0.105
u_{02}	−0.035	−0.035
T_{e0}	0.264	0.265
T_{i01}	0.061	0.06
T_{i02}	0.319	0.315

Note. All quantities are normalized.

V. CONCLUSION

Fluid algorithms for one-dimensional multi-fluid simulation of collisional plasmas have been presented and tested on a number of classical problems. Time-implicit computations of the electric field and of collision forces have been incorporated in the algorithms, allowing simulations over a wide range of the time-scale parameters $\omega_p \Delta t$ and $\nu_c \Delta t$. For $\omega_p \Delta t \gg 1$ (or $\nu_c \Delta t \gg 1$) the algorithms reduce to the quasi-static (or diffusion) approximations, but space-charge (and dynamical effects) are accurately represented in fluid regions where $\omega_p \Delta t \ll 1$ (and $\nu_c \Delta t \ll 1$). These algorithms are part of the development of hybrid simulations, which also include particles to represent plasma components requiring a kinetic treatment and hybrid simulations of diode closure, using the present fluid algorithms have been [redacted] resulting from exploding laser-heated CH foils [6]. These simulations were done with actual mass ratios (1836 and 22032) and include the streaming velocities in the computation of the collision frequencies. These simulations show that the plasma does not retain a fixed composition of carbon and hydrogen, as would occur in single-fluid codes. Such changes in composition modify the collisional damping of plasma waves and may have a significant effect on instability thresholds.

APPENDIX A: COLLISION COEFFICIENTS AND HEAT CONDUCTIVITIES

This appendix defines the collision frequencies and heat conductivities which enter in Eqs. (3) and (6). Two models,

rigid elastic spherical molecules and Coulomb interactions, which are used in the tests of Section IV, are considered.

1. *Collision Frequencies*

For rigid elastic spherical molecules, a simple geometrical argument gives

$$\nu_{ss'} = \pi\sigma_{ss'}^2 \langle v_{ss'}^2 \rangle^{1/2} n_{s'}, \tag{A1}$$

where $\sigma_{ss'}$ is the average diameter of the molecules, $n_{s'}$ is the density of species s', and

$$\langle v_{ss'}^2 \rangle^{1/2} = \left[\frac{T_s}{m_s} + \frac{T_{s'}}{m_{s'}}\right]^{1/2} \tag{A2}$$

is the "binary" thermal velocity. Equations (A1) and (A2) are written in cgs units. When written in normalized units, these equations give

$$\nu_{ss'} = C_{ss'} n_{s'}, \tag{A3}$$

where

$$C_{ss'} = \nu_0 \left[\frac{T_s}{m_s} + \frac{T_{s'}}{m_{s'}}\right]^{1/2}$$

and $\nu_0 = \pi\sigma_{ss'}^2 n_0 \lambda_0$. The collision parameters $C_{ss'}$ enter in the temperature equilibration term of Eq. (6). The collisional force also includes numerical constants $\alpha_{ss'}$ of order unity, which can be found from Chapman–Enskog theory [10], but these constants do not affect the algorithm and have been set to unity in the tests of Section IV.

For Coulomb interactions, the Chapman–Enskog theory or the Braginskii theory give, in Gaussian cgs units,

$$\nu_{ss'} = \frac{8}{3}\sqrt{\frac{\pi}{2}} \frac{\Lambda_{ss'} e_s^2 e_{s'}^2 n_{s'}}{\sqrt{m_{ss'}}\, T_{ss'}^{3/2}}, \tag{A4}$$

where $\Lambda_{ss'}$ is the Coulomb logarithm, $m_{ss'} = m_s m_{s'}/(m_s + m_{s'})$, and $T_{ss'} = m_{ss'} \langle v_{ss'}^2 \rangle$. In normalized units, Eq. (A4) gives $\nu_{ss'} = C_{ss'} n_{s'}$, where

$$C_{ss'} = \frac{1}{3}\sqrt{\frac{2}{\pi}}\, \Omega_p^2 r_0 \frac{\Lambda_{ss'} q_s^2 q_{s'}^2}{\sqrt{m_{ss'}}\, T_{ss'}^{3/2}} \tag{A5}$$

and $r_0 = e^2/(T_0 \lambda_0)$ is the normalized impact parameter for strong interaction ($\approx 90°$ deflection angle). The parameter r_0 defines the collisionality of the plasma. All quantities in Eq. (A5) are in normalized units. As in the case of rigid elastic spherical molecules, the constants $\alpha_{ss'}$ in the collision force have been set to unity in the tests of Section IV. In addition, the Coulomb logarithms $\Lambda_{ss'}$ are held constant for these tests.

2. *Heat Conductivities*

The heat flux in a given species is $-\kappa_s \nabla T_s$, where κ_s is the heat conductivity of that species. It is convenient to express the heat resistivity, κ_s^{-1}, as a sum of contributions from binary collisions with all species, $\kappa_{ss'}^{-1}$, plus a "vacuum contribution" κ_{s0}^{-1} which limits the heat flux for low collision rates.

$$\kappa_s^{-1} = \kappa_{s0}^{-1} + \sum_{s'} \kappa_{ss'}^{-1}.$$

The collisional contributions are found by simple geometrical arguments,

$$\kappa_{ss'}^{-1} = \frac{1}{\gamma_{ss'}} \frac{m_{ss'}}{T_s n_s} \nu_{ss'}, \tag{A6}$$

where $\gamma_{ss'}$ are numerical constants set to unity in the tests of Section IV.

The contribution κ_{s0}^{-1} is obtained by stating that in the collisionless case, the heat flux is

$$\kappa_{s0} |\nabla T_s| = f_s v_{\text{th}s} n_s T_s,$$

where $v_{\text{th}s} = (T_s/m_s)^{1/2}$ is the thermal velocity of species s and f_s is the flux-limiter coefficient, whence

$$\kappa_{s0}^{-1} = \frac{m_s^{1/2}}{f_s n_s} \frac{|\nabla T_s|}{T_s^{3/2}}. \tag{A7}$$

The form of Eqs. (A6) and (A7) are unchanged when expressed in normalized units.

APPENDIX B: TRANSPORT ALGORITHM

In the examples given in Section IV, density, momentum, and energy have been transported on the Eulerian mesh using Roe's "min-mod" limiter [11]. This flux limiter uses only values at the "old" time, giving better convergence of the electric field solver than FCT limiters, which also depend on values at the "new" time, and has been found to give better results at vacuum boundaries than the method of Van Leer. Both FCT and Van Leer limiters were studied in Ref. [1].

A single transport step, denoted in Eq. (7) by the operator Ψ,

$$n_j^t = \Psi\,[n_j^0, u_{j+1/2}^t],$$

is the result of adding and subtracting fluxes $f_{j-1/2}$ and $f_{j+1/2}$ from the adjacent cells,

$$n_j^t = n_j^0 - f_{j+1/2} + f_{j-1/2}.$$

Using Roe's min-mod limiter, the fluxes $f_{j+1/2}$ are computed as

$$f_{j+1/2} = [n_j^0 + \tfrac{1}{2}(1-\varepsilon_{j+1/2})\, n_j^*]\, \varepsilon_{j+1/2} \quad \text{if} \quad \varepsilon_{j+1/2} \geqslant 0$$
$$= [n_{j+1}^0 - \tfrac{1}{2}(1+\varepsilon_{j+1/2})\, n_{j+1}^*]\, \varepsilon_{j+1/2} \quad \text{if} \quad \varepsilon_{j+1/2} < 0,$$

where

$$n_j^* = 0 \quad \text{if} \quad [n_{j+1}^0 - n_j^0][n_j^0 - n_{j-1}^0] < 0$$
$$n_j^* = \text{sign}[n_{j+1}^0 - n_j^0] \times \text{Min}[|n_{j+1}^0 - n_j^0|, |n_j^0 - n_{j-1}^0|] \quad \text{otherwise}$$

and $\varepsilon_{j+1/2} = \Delta t\, u_{j+1/2}/\Delta x$.

ACKNOWLEDGMENT

This work is performed under the auspices of the U.S. Department of Energy by Lawrence Livermore National Laboratory under Contract W-7405-Eng-48.

REFERENCES

1. P. W. Rambo and J. Denavit, *J. Comput. Phys.* **92**, 185 (1991).
2. J. Denavit, "Time-Implicit Simulation of Particle-Fluid Systems," in *Space Plasma Simulation*, edited by M. Ashour-Abdalla and D. A. Dutton (Reidel, Boston, 1985), p. 85.
3. R. J. Mason, "Hybrid and Collisional Implicit Plasma Simulation Models," in *Multiple Time Scales*, edited by J. U. Brackbill and B. I. Cohen (Academic Press, New York, 1985), p. 233, and references cited there.
4. J. Denavit and P. W. Rambo, "Algorithms for Time-Implicit Collisional Plasma Simulation," in *Proceedings, 13th Conference on the Numerical Simulation of Plasmas, Santa Fe, NM, Sept. 17–20, 1989*, paper PW-14.
5. S. I. Braginskii, *Rev. Plasma Phys.* **1**, 205 (1965).
6. J. Denavit and P. W. Rambo, *Bull. Am. Phys. Soc.* **35**, 1932 (1990).
7. Ya. B. Zel'dovich and Yu. P. Raizer, *Physics of Shock Waves and High-Temperature Hydrodynamic Phenomena* (Academic Press, New York, 1966), p. 49.
8. Ya. B. Zel'dovich and Yu. P. Raizer, *ibid.*, p. 515.
9. V. D. Shafranov, *J. Exp. Theoret. Phys. (U.S.S.R.)* **32**, 1453 (1957); *JETP* **5**, 1183 (1957).
10. S. Chapman and T. G. Cowling, *The Mathematical Theory of Non-Uniform Gases* (Cambridge Univ. Press, New York, 1960).
11. P. K. Sweby, *SIAM J. Numer. Anal.* **21**, 995 (1984).